Advances in the Theory of Nonlinear Analysis and its Applications 7 (2023) No. 4, 99-113.
https://doi.org/10.17762/atnaa.v7.i4.286
Available online at www.https://atnaea.org/
Research Article

Advances in the Theory of Nonlinear Analysis and its Applications
ISSN: 2587-2648
Peer-Reviewed Scientific Journal

The Influence of the Magnetic Domain on The Peristaltic Motion of The Non-Newtonian Fluid in A Curved Tube

Farah Alaa Adnan[a], Aya Hadi AlHaddad[a], Zainab Abdulkareem Abed Ali[a], Manar Naji Ghayyib[a]

[a] *Department of Mathematics, College of Science, University of Baghdad, Baghdad, Iraq.*

Abstract

The peristaltic pump of a fluid which is of non-Newtonian type over a curved tube is the main focus of this study. The mathematical formulation of the problem is presented. A small Reynolds number (Re) and a large wavelength (δ) are used to simplify the calculation of the problem. The final expression of the stream function is found by applying the perturbation procedure for different values k, we derive a numerical solution to the nonlinear differential equation. An extensive review of the influence of various physics parameters, such that Hartman number, non-Newtonian fluid number and many others, in two cases, small and large values of the curvature value k, on the axial velocity profile, the pressure rise, the pressure gradient, and the streamlines. This discussion is supported by the inclusion of pictures and illustrations.

Keywords: Peristaltic motion; Non-Newtonian fluid; Curved tube; Magnetic field; Trapping.
2010 MSC: 76Axx, 76Mxx.

1. Introduction

The continual stretching and loosening of muscle in the digestive tract are called peristalsis, and it is responsible for the downward movement of food. Recent interest in the peristalsis phenomenon can be attributed to engineering and medical uses. Embryonic development, the transport of oocytes and embryos, and the pulsation of blood arteries are all examples of peristaltic flow in living systems [1, 2, 3, 4, 5, 6, 7, 8, 9, 10, 11, 12, 13]. One advantageous component in engineering applications is turbo machines and aircraft wings.

Email address: farah.alaa@sc.uobaghdad.edu.iq (Farah Alaa Adnan)

Received September 24, 2023; Accepted: November 25, 2023; Online: December 20, 2023.

Consequently, it is of most importance to comprehend the impact of curvature (represented by the variable k) on the behavior of channels. The investigation of peristaltic movements in curvy channels holds significant academic interest due to the prevalence of curved shapes in physiological tubes and glandular channels. The phenomenon of flow in a curved tube holds significant relevance in several industrial, biological, and environmental contexts. The dispersion of pollutants within fjords and across rugged maritime topography exemplifies the phenomenon of flow in curved channels. Laser droving in curved plasma channels is crucial in many types of laser systems, including circular x-ray lasers, optical synchrotrons, accelerators, and generating harmonic lasers. Additionally, from an engineering perspective, the properties of flood flow in relation to the movement of sediments are an application of curved geometry [14, 15, 16, 17, 18, 19, 20, 21, 22, 23, 24, 25]. Because of its usefulness in a wide variety of contexts, including food mixing, chime movement in the intestine, blood and plasma flow, and the distribution of unclear fuel slurries, the study of non-Newtonian fluids flow has attracted the attention of many researchers. Shear stress and shear strain in Bingham plastic materials are linear, and a finite yield stress is necessary for the fluid starting to flow[26, 27, 28, 29, 30]. Drilling mud, toothpaste, clay suspension, mayonnaise, chocolate, and mustard are just few of the many uses for Bingham plastic fluid. In contrast to Newtonian fluids, whose fixed surface is flat and featureless, the Bingham plastic fluid's surface can hold spikes [31, 32, 33, 34, 35]. A research was done by Adana and Hadi to examine the influence of a field of magnetic particles on the peristaltic pumping behavior of a Bingham plastic fluid within an inclined balanced duct. Additionally, the study took into account the impacts of heat transfer and mass transfer [36]. The peristaltic flow of an incompressible Bingham plastic fluid in a curved duct was investigated by Adnan [37]. Trinary hybrid nanofluid flow was investigated by Z. Abbas et al. between two sinusoidally deflected curved tubes [38]. The impacts of a magnetic field on the peristaltic movement of Bingham fluid were examined in a study by Adnan [39]. In their study, Al-Khafajy and Labban examined the collective impacts of concentration and thermo-diffusion on the dynamics of unstable oscillatory flow in an inclined porous channel, specifically focusing on an incompressible Carreau fluid [40]. Nazeer conducted a comparative analysis on the two-dimensional cross flow of a non-Newtonian fluid with heat and mass transfer. Specifically, the focus was on the Eyring-Powell fluid, which was observed while it flowed through a uniform horizontal channel [41]. The theoretical examination conducted by Kotnurkar et al. focuses on the significance of double-diffusive convection involving magneto-Jeffrey nanofluid in a peristaltic motion. This examination takes into account the influence of magnetohydrodynamics (MHD) and a porous medium within a flexible channel with a permeable wall [42]. The effects of rotation on heat transport for a couple-stress within a non-uniform canal were studied by Abdulhussein et al. utilizing inclination magnetohydrodynamics [43]. The Bingham plastic material model is a suitable approach for accurately representing the rheological characteristics of several lubricants employed in hydrodynamic bearings. The observed behavior exhibits a distinct transition, wherein the material undergoes a transformation from a solid state to a fluid state, contingent upon the magnitude of the shear stress experienced at a given location [44]. The effect of magnetic force and nonlinear thermal radiation for peristaltic transport of hybrid bio-nanofluid with the porous medium in a symmetric channel [45]. A computational study was performed to investigate the slip and no-slip possibilities for the flow of a Bingham fluid in a spiral tube with a circular cross-section [46]. The numerical investigation of the flow of Bingham plastic fluid on a heated rotating disc is presented by Khan et al., thermo-physical characteristics and viscous dissipation are postulated with the influence of entropy formation [47].

Samanta et al. conducted a study to analyse the hydrodynamics of a laminar planar hydraulic jump occurring during the free surface flow of a Bingham plastic liquid. The researchers employed numerical simulation and shallow flow analysis techniques, which were subsequently validated using experimental data [48]. Mohammed examines the impact of the rotation variable and other variables on the peristaltic flow of Sutterby fluid in an inclined asymmetric channel that includes a porous material with heat transfer. When there is rotation, mathematical modelling is created by employing constitutive equations that are based on the Sutterby fluid model [49]. Mohammed studies the influence of the rotation variable on the peristaltic movement of Sutterby fluid in an asymmetric channel with thermal transfer. The mathematical representation incorporates the influence of rotation by employing constitutive equations basing on the

Sutterby fluid model [50].

2. The Formulation of the Problem

Non-Newtonian fluid fills the space inside the tube; hence the problem is formulated as peristaltic motion of an incompressible non-Newtonian fluid through curved pipe with a width of (2a) becomes intricate in an annular circle with a center of 0 and a radius of R^*. Defining $\bar{V}$ and $\bar{U}$ are the variables of velocity in radial $\bar{R}$ and axial $\bar{X}$ direction respectively as it is showing in figure 1. The mathematical description of the tube sidewalls proceeds as the following:

$$\mp\bar{H}\left(\bar{X},\ \bar{t}\right) = \mp\left[a + b\left[\frac{2\pi}{\lambda}\left(\bar{X} - c\bar{t}\right)\right]\right] \tag{1}$$

In this context, a variable c represents the speed, the wave amplitude of the upper sidewall and lower side wall are denoted by b. The wavelength, which is represents by λ, represents has decreased in smaller increments, but in more practical scenarios, Natural systems contraction and expansion cause time variations. which is influenced by fluctuating values of λ. In order to treat the flow in a curved channel as two-dimensional, it is assumed that the breadth perpendicular to the plane of the tube is infinitely large. It is believed that the motion is moving through a laminar state. Based on the aforementioned premise, we consider the field of motion to have the form that is shown below.

$$\bar{V} = \left[\bar{V}\left(\bar{R},\bar{X},\bar{t}\right),\bar{U}\left(\bar{R},\bar{X},\bar{t}\right),0\right]$$

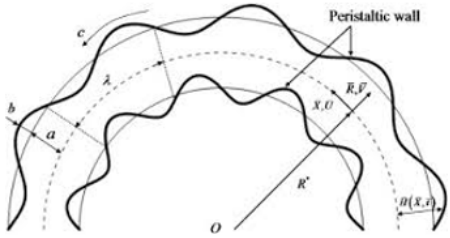

Figure 1: The design of tube

For the velocity field of an incompressible, non-Newtonian fluid, the equations that account for mass and momentum conservation are shown below:

$$\nabla.\bar{V} = 0 \tag{2}$$

$$\rho\left(\frac{\partial\bar{V}}{\partial t} + \left(\bar{V}.\bar{\nabla}\right)\bar{V}\right) = -\nabla\bar{P} + \nabla.\bar{\tau} - \sigma B_0^2\bar{V} \tag{3}$$

Defining the fluid density, the pressure, and the stress tensor by the symbols $\rho, \bar{P}$, and $\bar{\tau}$ respectively.

$$\rho\left(\frac{\partial\bar{V}}{\partial t} + \left(\bar{V}.\bar{\nabla}\right)\bar{V}\right) = -\nabla\bar{P} + \nabla.\bar{\tau} - \sigma B_0^2\bar{V} \tag{4}$$

$$\begin{aligned}\rho\left[\frac{\partial\bar{V}}{\partial\bar{t}} + \bar{V}\frac{\partial\bar{V}}{\partial\bar{R}} + \frac{R^*\bar{U}}{R^*+\bar{R}}\frac{\partial\bar{V}}{\partial\bar{X}} - \frac{\bar{U}^2}{R^*+\bar{R}}\right] &= -\frac{\partial\bar{P}}{\partial\bar{R}} + \frac{1}{R^*+\bar{R}}\frac{\partial}{\partial\bar{R}}\left[\left(R^*+\bar{R}\right)\bar{\tau}_{\bar{R}\bar{R}}\right] \\ &+ \left(\frac{R^*}{R^*+\bar{R}}\right)\frac{\partial\bar{\tau}_{\bar{R}\bar{X}}}{\partial\bar{X}} - \frac{\bar{\tau}_{\bar{X}\bar{X}}}{R^*+\bar{R}} - \sigma {B_0}^2\bar{V}\end{aligned} \tag{5}$$

$$\rho\left[\frac{\partial\bar{U}}{\partial\bar{t}}+\bar{V}\frac{\partial\bar{U}}{\partial\bar{R}}+\frac{R^*\bar{U}}{R^*+\bar{R}}\frac{\partial\bar{U}}{\partial\bar{X}}+\frac{\bar{U}\bar{V}}{R^*+\bar{R}}\right]=-(\frac{R^*}{R^*+\bar{R}})\frac{\partial\bar{P}}{\partial\bar{X}}+\frac{1}{(R^*+\bar{R})^2}\frac{\partial}{\partial\bar{R}}\left[(R^*+\bar{R})^2\bar{\tau}_{\bar{R}\bar{X}}\right]+\left(\frac{R^*}{R^*+\bar{R}}\right)\frac{\partial\bar{\tau}_{\bar{X}\bar{X}}}{\partial\bar{X}}\quad-\sigma{B_0}^2\bar{U} \tag{6}$$

Along with the boundary conditions:

$$\bar{U}=0 \text{ alongwith } \mp\bar{H}\left(\bar{X},\bar{t}\right)=\mp\left[a+b\ \sin\left[\frac{2\pi}{\lambda}\left(\bar{X}-c\bar{t}\right)\right]\right] \tag{7}$$

Cauchy stress tensor, denoted as σ^*, can be expressed in the following reduced form.

$$\sigma^*=-\bar{P}I+\bar{s}$$

The symbol $\bar{\tau}$ denotes the additional stress tensor, the symbol $\bar{P}$ represents the kinetic pressure. The non-Newtonian fluid stresses, denoted as s_{ij}, are connected to the strain rates $\bar{A}_1$ through the utilisation of a constitutive equation.
$\bar{s}_{ij}=(2\ \mu+\frac{s_y}{\dot{\bar{\gamma}}})\bar{A}_1$ for $\tau\geq\tau_y, \bar{s}_{ij}=0$ for $s<s_y$.
In which s_y indicates the yield stress and μ denotes the fluid viscosity,

$$\dot{\bar{\gamma}}=\left(\frac{1}{2}\ trac\bar{A}_1^2\right)^{\frac{1}{2}},\ \text{and}\ \bar{A}_1=grad\ \bar{V}+(grad\ \bar{V})^T$$

$$\dot{\bar{\gamma}}=\left(2\left(\frac{\partial\bar{V}}{\partial\bar{R}}\right)^2+\left(\frac{\partial\bar{U}}{\partial\bar{R}}+\frac{R^*}{R^*+\bar{R}}\frac{\partial\bar{V}}{\partial\bar{X}}-\frac{\bar{U}}{R^*+\bar{R}}\right)^2+2\left(\frac{R^*}{R^*+\bar{R}}\frac{\partial\bar{U}}{\partial\bar{X}}+\frac{\bar{V}}{R^*+\bar{R}}\right)^2\right)^{\frac{1}{2}}$$

The flow is irregular in the tube. Yet in the wave frame with coordinates $(\bar{r},\bar{x})$, which are moving with speed c, it seems stable. The following is an introduction to the equations of transformation:

$$\bar{x}=\bar{X}-c\bar{t},\bar{r}=\bar{R},\ \bar{u}=\bar{U}-c\ ,\bar{v}=\bar{V},\bar{P}=\bar{p} \tag{8}$$

For the purpose of determining the non-dimensional analysis, the dimensionless quantities required are shown below:

$$\begin{aligned}&x=\frac{2\pi\bar{x}}{\lambda},\ \eta=\frac{\bar{r}}{a},\ u=\frac{\bar{u}}{c},\ v=\frac{\bar{v}}{c},\\&p=\frac{2\pi a^2}{\lambda\mu c}\ \bar{p},h=\frac{\bar{H}}{a},\ \tau=\frac{a\bar{\tau}}{\mu c},Re=\frac{\rho ca}{\mu},\ \delta=\frac{2\pi a}{\lambda},\\&k=\frac{R^*}{a},\ \varphi=\frac{b}{a},\dot{\gamma}=\frac{\rho a^2}{\mu_0}\dot{\bar{\gamma}},M=\frac{\sigma{B_0}^2a^2}{\mu},\ N=\frac{a\ \tau}{\mu c}\end{aligned} \tag{9}$$

The non-dimensional components of velocity are represented by (u,v). The variable p is used to represent the non-dimensional pressure, And the symbol τ is used to represent the non-dimensional stress tensor. The Reynolds number, denoted as Re, is a numerical value that represents a dimensionless quantity in fluid mechanics. The symbol δ represents the wavelength ratio, also known as the wave number. On the other hand, the symbol k signifies the curvature parameter. The symbol φ represents the amplitude ratio, Hartman number, denoted by M. and the symbol N denotes the Non-Newtonian fluid number. Using these values, we could analyze the motion and continuity equations:

$$(k+\eta)\frac{\partial v}{\partial\eta}+k\delta\frac{\partial u}{\partial x}+v=0 \tag{10}$$

And the motion equation in $\bar{R}$ direction

$$-\delta^2Re\frac{\partial v}{\partial x}+Re\ \delta v\frac{\partial v}{\partial\eta}+Re\ \delta\frac{k\,(u+1)}{k+\eta}\frac{\partial v}{\partial x}-Re\ \delta\frac{(u+1)^2}{k+\eta}=-\frac{\partial p}{\partial\eta}+\frac{\delta}{k+\eta}\frac{\partial}{\partial\eta}\left[(k+\eta)\,\tau_{\eta\eta}\right]+\delta^2\left(\frac{k}{k+\eta}\right)\frac{\partial\tau_{\eta x}}{\partial x}-\delta\frac{\tau_{xx}}{ak+a\eta}-\delta\ Mv \tag{11}$$

And the motion equation in $\bar{X}$ direction

$$-Re\delta\frac{k+\eta}{k}\frac{\partial u}{\partial x}+Re\frac{k+\eta}{k}v\frac{\partial u}{\partial \eta}+Re\delta\left(u+1\right)\frac{\partial u}{\partial x}+Re\frac{\left(u+1\right)v}{k}=-\frac{\partial p}{\partial x}+\frac{1}{k}\frac{1}{k+\eta}\frac{\partial}{\partial \eta}\left[\left(k+\eta\right)^{2}\tau_{\eta x}\right]+\delta\frac{\partial \tau_{xx}}{\partial x}-\frac{k+\eta}{k}M(u+1) \tag{12}$$

Along with non-dimensional boundary conditions

$$u+1=0,\mp[h]=\mp\left[1+\varphi\sin x\right] \tag{13}$$

And the stream function

$$u=-\frac{\partial \psi}{\partial \eta} \tag{14}$$

Using the Eq. (14) in the Eq. (13), one obtains

$$-\frac{\partial \psi}{\partial \eta}+1=0$$

Then the boundary conditions

$$\frac{\partial \psi}{\partial \eta}=1,\mp[h]=\mp\left[1+\varphi\sin x\right] \tag{15}$$

$$\dot{\gamma}=\left(2\ Re^{2}\left(\frac{\partial v}{\partial \eta}\right)^{2}+\left(\ Re\frac{\partial u}{\partial \eta}+\ \delta\ Re\frac{k}{k+\eta}\frac{\partial v}{\partial x}-\ Re\frac{(u+1)}{k+\eta}\right)^{2}+2\left(\delta\ Re\ \frac{k}{k+\eta}\frac{\partial u}{\partial x}+\ Re\frac{v}{k+\eta}\right)^{2}\right)^{\frac{1}{2}}$$

A small Reynolds number (Re) and a large wavelength (δ) are used to simplify the calculation. The solution to the governing equations may be determined, and the equations in the question representable as

$$\frac{\partial p}{\partial \eta}=0 \tag{16}$$

$$\frac{\partial p}{\partial x}=\frac{1}{k}\ \frac{1}{k+\eta}\frac{\partial}{\partial \eta}\left[(k+\eta)^{2}\tau_{\eta x}\ \right]-\frac{k+\eta}{k}M(-\frac{\partial \psi}{\partial \eta}+1) \tag{17}$$

Also

$$\dot{\gamma}=\ Re(-\frac{\partial^{2}\psi}{\partial \eta^{2}}-\ \frac{1}{k+\eta}\left(1-\frac{\partial \psi}{\partial \eta}\right)),$$

but

$$\bar{\tau}_{ij}=\left(2\mu_{0}+\frac{\tau_{y}}{\dot{\bar{\gamma}}}\right)\bar{A}_{1},$$

then

$$\tau_{\eta x}=\left(2+\frac{\rho a^{2}\tau_{y}}{{\mu_{0}}^{2}\gamma}\right)\left(\ \frac{\partial u}{\partial \eta}-\ \frac{u+1}{k+\eta}\right)$$

$$\tau_{\eta x}=2\left(-\ \frac{\partial^{2}\psi}{\partial \eta^{2}}-\ \frac{1}{k+\eta}(1-\frac{\partial \psi}{\partial \eta})\right)+N,$$

then

$$\frac{\partial p}{\partial x}=\frac{1}{k}\ \frac{1}{k+\eta}\frac{\partial}{\partial \eta}\left[(k+\eta)^{2}\left(2\left(-\ \frac{\partial^{2}\psi}{\partial \eta^{2}}-\ \frac{1}{k+\eta}\left(1-\frac{\partial \psi}{\partial \eta}\right)\right)+N\right)\ \right]-\frac{k+\eta}{k}M(-\frac{\partial \psi}{\partial \eta}+1) \tag{18}$$

Deriving the above equation with respect to η and doing more simplification

$$\frac{\partial^{4}\psi}{\partial \eta^{4}}+\frac{2}{(k+\eta)}\frac{\partial^{3}\psi}{\partial \eta^{3}}-\frac{1}{(k+\eta)^{2}}\frac{\partial^{2}\psi}{\partial \eta^{2}}+\left(\frac{\partial \psi}{\partial \eta}-1\right)\frac{1}{(k+\eta)^{3}}-\frac{M}{2}\frac{\partial^{2}\psi}{\partial \eta^{2}}-\frac{M}{2(k+\eta)}\left(\frac{\partial \psi}{\partial \eta}-1\right)=0 \tag{19}$$

3. The solution of This Problem

Using the perturbation method by expanding the stream function:

$$\psi = \psi_0 + \frac{1}{k}\psi_1 + \frac{1}{k^2}\psi_3$$

$$\frac{1}{k+\eta} = \frac{1}{k} - \frac{\eta}{k^2} + \frac{\eta^2}{k^3}$$

$$\frac{1}{(k+\eta)^2} = \frac{1}{k^2} - \frac{2\eta}{k^3} + \frac{3\eta^2}{k^4}$$

$$\frac{1}{(k+\eta)^3} = \frac{1}{k^3} - \frac{3\eta}{k^4} + \frac{6\eta^2}{k^5} \tag{20}$$

Substituting the above series (20) with the Eq. (19) then the solution

$$\begin{aligned}
\psi = {} & \frac{2e^{-\frac{\sqrt{M}\eta}{\sqrt{2}}}\left(e^{\sqrt{2}\sqrt{M}\eta}A_1 + A_2\right)}{M} + A_3 + \eta * A_4 + (1/k)\left(A_7 + \eta A_8 + \left(-\left((-1+A_4)M^{\frac{3}{2}}\eta^2\right.\right.\right. \\
& + e^{-(\sqrt{M}\ \eta)/\sqrt{2}}\left(-5\sqrt{2}A_2 - 2A_2\sqrt{M}\ \eta + 4\sqrt{M}\ A_6\right) \\
& \left.\left.\left. + e^{(\sqrt{M}\ \eta)/\sqrt{2}}\ (5\sqrt{2}\ A_1 + 4\sqrt{M}\ A_5\ - 2\sqrt{2}A_1\ Log[e^{(\sqrt{M}\ \eta)/\sqrt{2}}])\right)/\left(2\ M^{\frac{3}{2}}\right)\right) \right. \\
& + (1/k^2)\left(A_{11} + \eta A_{12} + \frac{1}{8}\left(-4(-1+A_8)\eta^2 + \frac{8}{3}(-1+A_4)\eta^3\right.\right. \\
& + \frac{e^{-\frac{\sqrt{M}\eta}{\sqrt{2}}}(-4A_6(5\sqrt{2}\sqrt{M} + 2M\eta) + 6\ A_2(2 + 2\sqrt{2}\sqrt{M}\eta + M\eta^2) + 16MA_{10})}{M^2} \\
& + (2e^{(\sqrt{M}\ \eta)/\sqrt{2}}\ )\ (10\sqrt{2}\ A_5\sqrt{M} - 4\ A_5M\eta + A_1(6 - \sqrt{2}\ \sqrt{M}\ \eta + M\eta^2) \\
& \left.\left. + 8M\ A_9 + 2\ A_1(-5 + \sqrt{2}\ \sqrt{M}\ \eta)Log[\ e^{(\sqrt{M}\ \eta)/\sqrt{2}}])\right)/M2\right)\Bigg)
\end{aligned}$$

The rate of volume flow can be expressed as

$$F = -\int_{-h}^{h} \frac{\partial\psi}{\partial\eta} d\eta = -\left(\psi\left(h\right) - \psi\left(-h\right)\right)$$

And

$$\psi\left(h\right) - \psi\left(-h\right) = -F$$

Then at the upper sidewall of the tube $\psi\left(h\right) = -\frac{F}{2}$ and at the lower sidewall of the tube $\psi\left(-h\right) = \frac{F}{2}$. Numerical computation of the dimensionless pressure rise over a single wavelength is performed using the following equation.

$$\Delta p_\lambda = \int_0^{2\pi} \frac{dp}{dx}\ dx$$

4. The Analysis

In this section, we saw a visual representation of how various variables impact the final flow principles. Graphical representations and analyses of changes the different variables in axial velocity, on the pressure gradient, on the pressure rise, and on the stream lines are shown.

4.1. The velocity profile

The velocity profile is visually shown by graphical analysis in the next Figures 2-7. The figures indicate that the axial velocity displays a parabolic pattern.

Figure 2 illustrates the variation in velocity as the value of the parameter η rises. That velocity profile seems to grow with increasing of η except when $\eta = 0$. For small values of k, Figure 3 describes the velocity behaver for different value of the curvature parameter. The velocity profile is not symmetric and increasing is some area and declines in another one. However, in Figure 4 the axial velocity attains to be symmetric and fixed for large values of the curvature parameter. The association between the flow rate F and velocity profile is illustrated in Figure 5. The velocity profile rises in the middle part of the tube and falls at inner and outer sides of its.

Figure 6 depicts the velocity profile for various Hartman numbers. It has been shown that the axial velocity grows with larger values of M. Figure 7 illustrates the velocity profile for increasing values of the amplitude ratio parameter, which is denoted by as ϕ. The velocity profile shows a reduction towards the central region of the tube, while it shows an increase towards both the inner and outer walls of the tube.

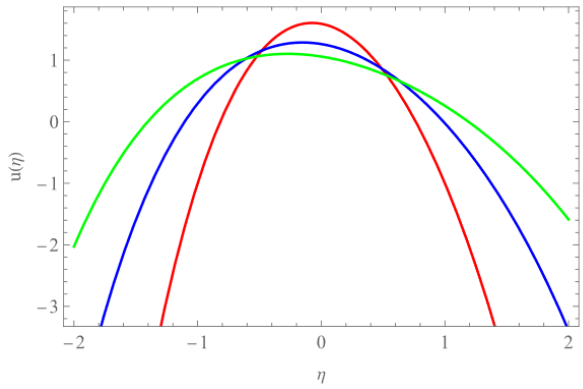

Figure 2: The velocity profile for η with k=5, ϕ=0.5, F=1, M=1.

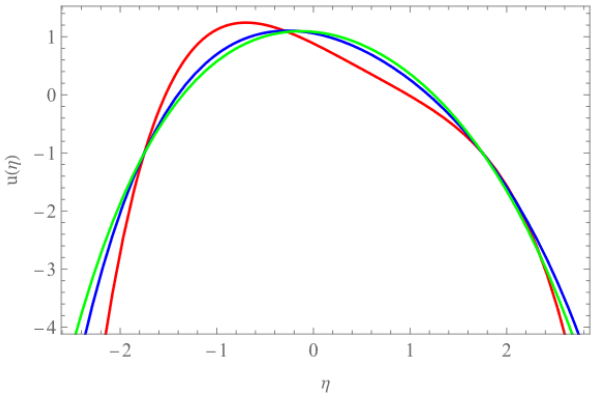

Figure 3: The velocity profile for k=2,5,10 with ϕ=0.5, F=1, M=1.

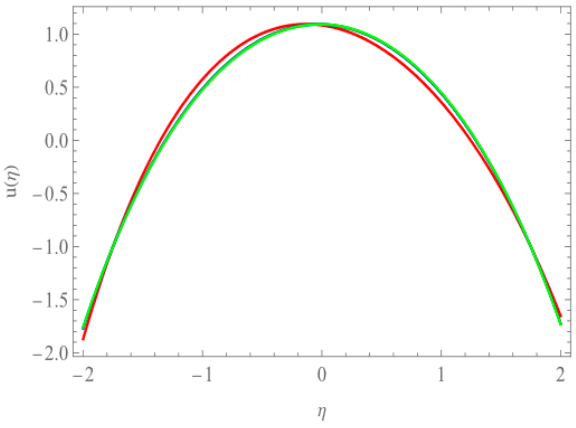

Figure 4: The velocity profile for k=10, 50, 75 with ϕ=0.5, F=1, M=1

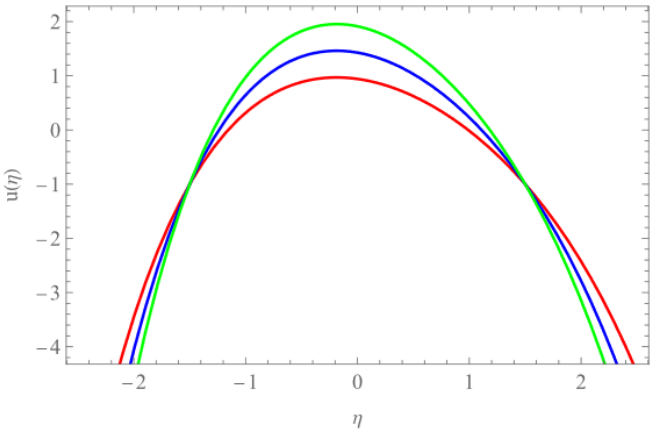

Figure 5: The velocity profile for F=1,1.5,2 with k=5, ϕ=0.5, M=1.

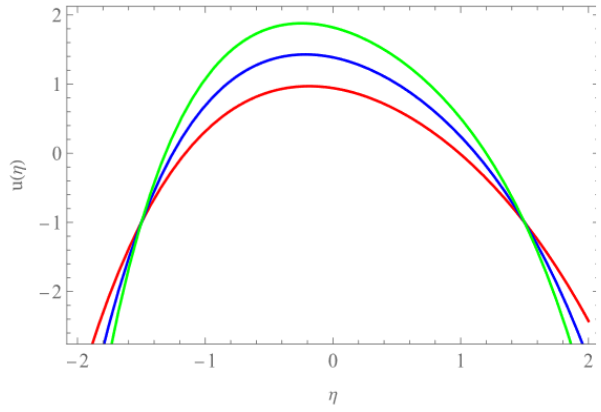

Figure 6: The velocity profile for M=1,2,3 with k=5, ϕ=0.5, F=1.

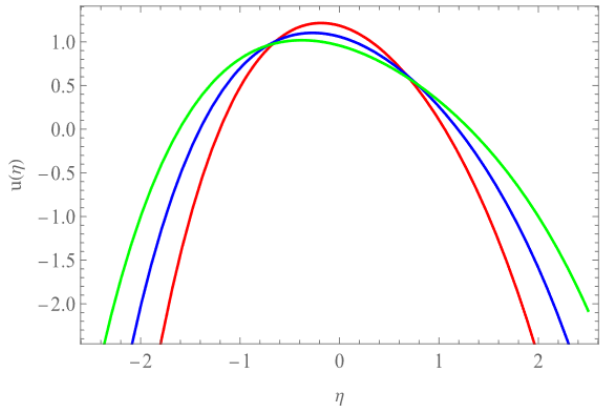

Figure 7: The velocity profile for ϕ=0.5, 0.75, 1 with k=5, F=1, M=1.

4.2. The pressure gradient $(\frac{\partial p}{\partial x})$

Figure (8-12) shows the behavior of the pressure gradient $(\frac{\partial p}{\partial x})$ for different values such that the curvature parameter, the flow rate, amplitude ratio parameter, the non-Newtonian fluid number and the Hartman number. These graphs show that the pressure gradient oscillates along the side walls of the tube. Figure 8 shows that $\frac{\partial p}{\partial x}$ exhibits a rise when considering small values of the curvature parameter k . The impact of the flow rate on the $(\frac{\partial p}{\partial x})$ is presented in Figure 9. It can be seen how the pressure gradient falls when the value of F grows. Figure 10 illustrates the variations in the pressure gradient as the amplitude ratio parameter ϕ increases. The given case illustrates a rise in the pressure gradient. The visual outcomes of the pressure gradient for the Non-Newtonian fluid number are depicted in Figure 11. The pressure gradient fixed with an increase of N. As illustrated in Figure 12, the pressure gradient declines as the Hartman number rises.

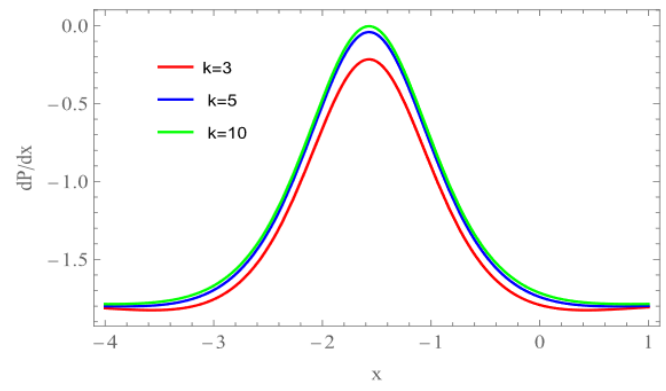

Figure 8: The pressure gradient for k=3,5,10 with F=1, ϕ=0.5, N=25, M=1.

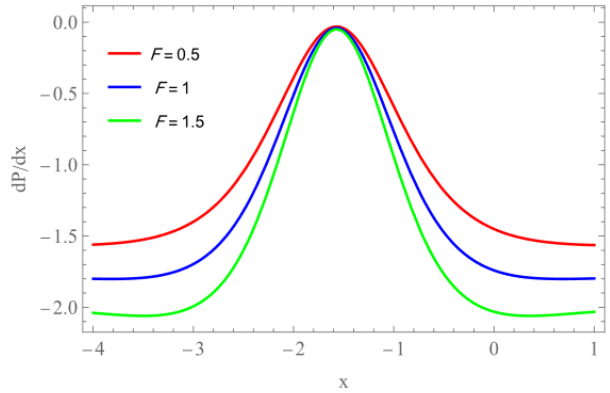

Figure 9: The pressure gradient for, F=0.5,1,1.5 with k=5, ϕ=0.5, N=25, M=1.

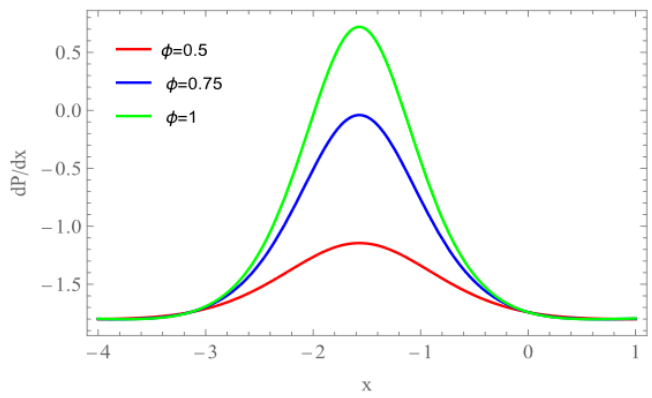

Figure 10: The pressure gradient for ϕ=0.5,0.75,1 with k=5, F=1, N=25, M=1.

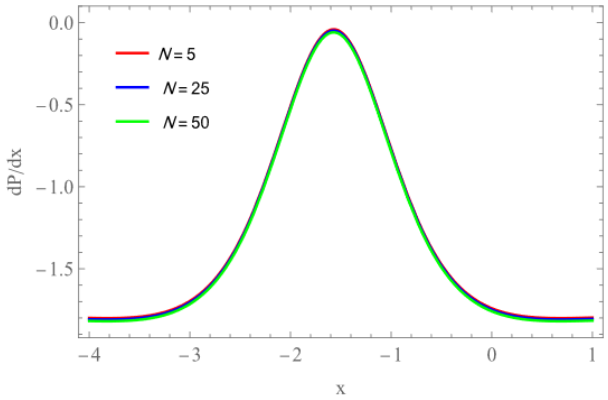

Figure 11: The pressure gradient for N=5,25,50 with k=5, F=1, ϕ=0.5, M=1.

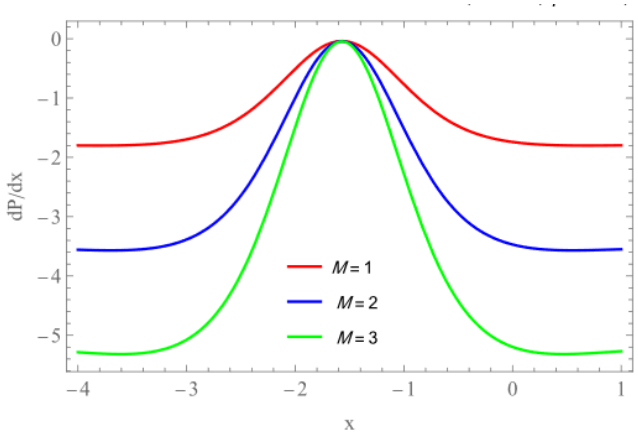

Figure 12: The pressure gradient for M=1,2,3 with k=5, F=1, ϕ=0.5, N=5.

4.3. The pressure rise

The connection between the non-dimensional average pressure rise per wavelength and the dimensionless mean rate of flow is the interest in this context. The investigation of Θ is carried out for various values of the physical parameter. The impact of rising the value of curvature parameter, which is denoted by k, on the pressure rise is displayed in Figure 13. The pressure rise per wave length verses flow rate Θ declines with an increase of k in the region $\Delta p > 0, \Theta > 0$ and increase in the co- pumping region where $\Delta p < 0, \Theta < 0$. Figure 14 is plotted to see the effect of various growing values of amplitude ratio parameter, which is denoted by ϕ, on the pressure rise. The pressure rise decrease is observed in the co-pumping area, whereas pressure rise is observed in the free pumping region, where the change $\Delta p = 0$. Figure 15 has been devised to examine the relationship between pressure rise and the increase of the non-Newtonian fluid number. It is evident that is the pressure rise followed by a period of stability. Figure 16 depicts the impact of the Hartman number on the pressure rise. It has been observed that there is an increase in pressure rise for rising values of M in the free pumping region, where $\Delta p = 0$. Conversely, there is a drop-in pressure rise in the co-pumping region.

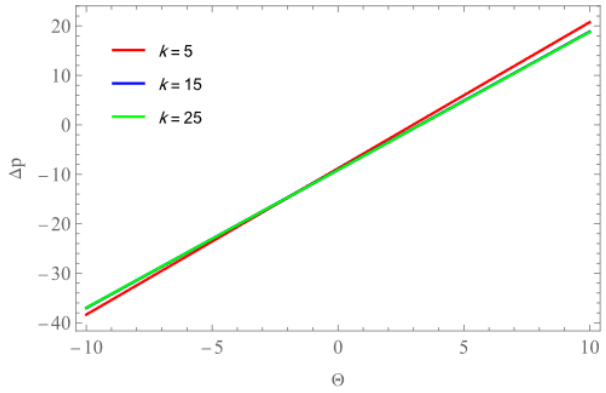

Figure 13: The pressure rise for k=5,15,25 with ϕ=0.5, N=5, M=1.

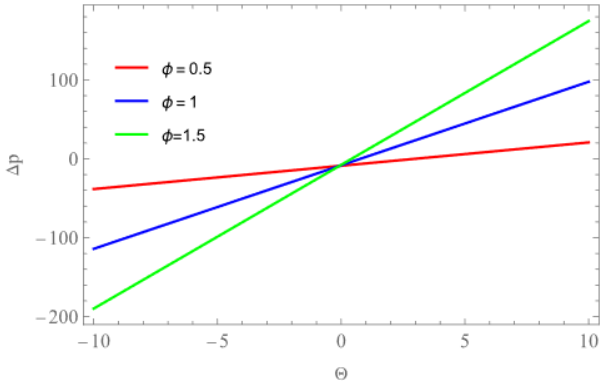

Figure 14: The pressure rise for ϕ=0.5,1,1.5 with k=5, N=5, M=1.

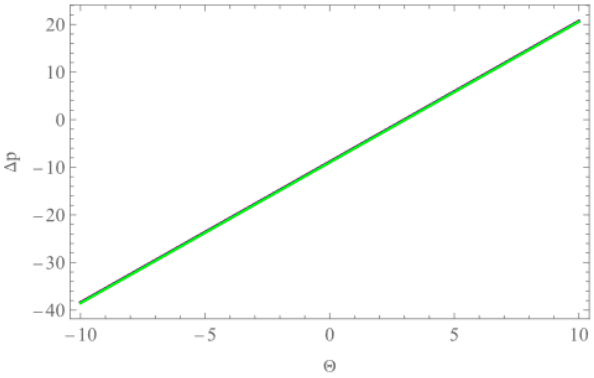

Figure 15: The pressure rise for N=5,10,15 with k=5, ϕ=0.5, M=1.

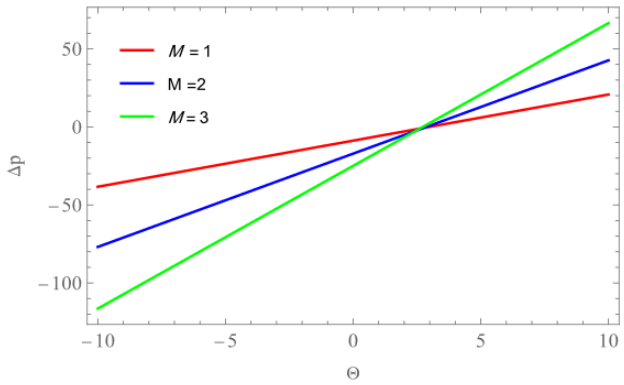

Figure 16: The pressure rise for M=1,2,3 with k=5, ϕ=0.5, N=5.

The trapping phenomenon holds significant importance in the context of peristaltic motion. The trapping phenomenon is caused by the circulation and separation of fluid bolus streamlines, which reveal a narrow formation. Figure (17-23) display the generation of trapped bolus for the flow. For varying values of the curvature parameters, as shown in Figure 17, the bolus or circulation region separates into two boluses, one in the lower half and one in the upper half of the tube. When k is small, as in (a) the boluses are not symmetric in shape and size around the center and conversely in (b), (c) for large values of k, the boluses are symmetric in shape and size around the center. Figures 18 and 19 are set up to observe how the stream lines behaves under the increase of amplitude ratio parameter. For both high and small values of k, the streamlines break off into two asymmetric boluses at the center, with the boluses becoming bigger as ϕ increases. Figure 20 displays the streamlines corresponding to high values of the parameter k, illustrating the effect of raising the flow rate F on the streamlines. The results indicate that the streamlines separate into two distinct boluses within the lower and upper regions of the curved tube. These boluses exhibit symmetrical characteristics in terms of shape and size, with their sizes proportionally increasing alongside the increase of F. While Figure 21 demonstrates that the boluses in the lower and upper of the curved tube are not symmetric in shape and size by increasing the value of F for small values of k. Figure 22 shows that by increasing the value of the Hartman number when k is quite big, the boluses are not symmetric in shape and size in the upper and lower parts of the tube, and the boluses shrink. Figure 23 shows that the boluses keep their size and symmetry in the upper half of the tube by increasing the value of the Hartman number for small values of k.

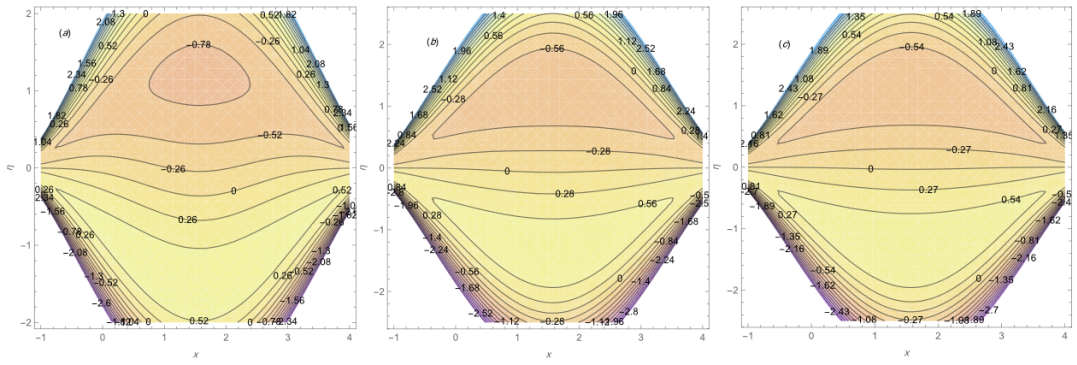

Figure 17: The stream lines for k=5,10,25 with ϕ=1, F=1, M=1.

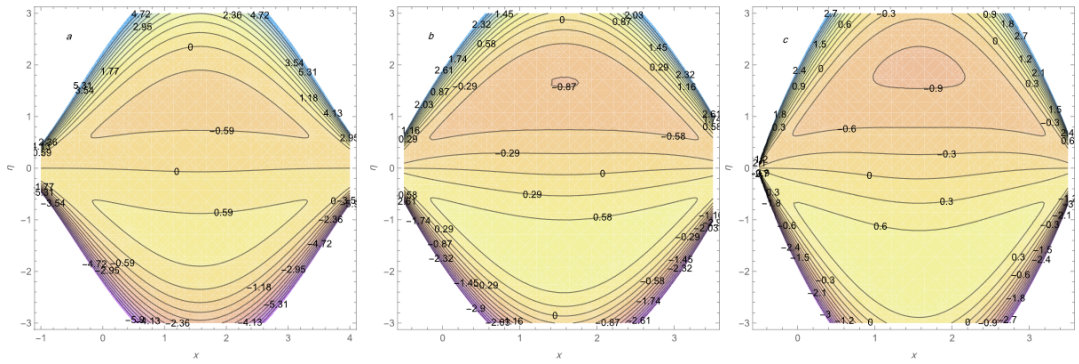

Figure 18: The stream line for ϕ=1,1.5,2 with k=25, F=1, M=1.

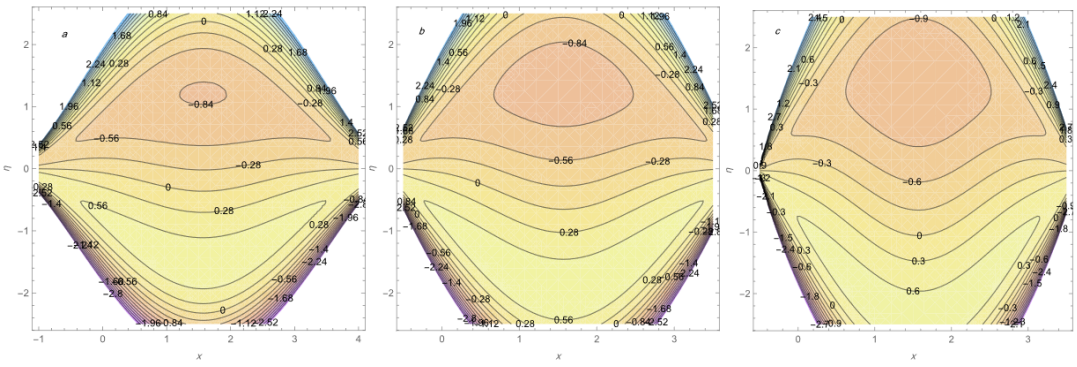

Figure 19: The stream line for ϕ=1,1.5,2 with k=5, F=1, M=1.

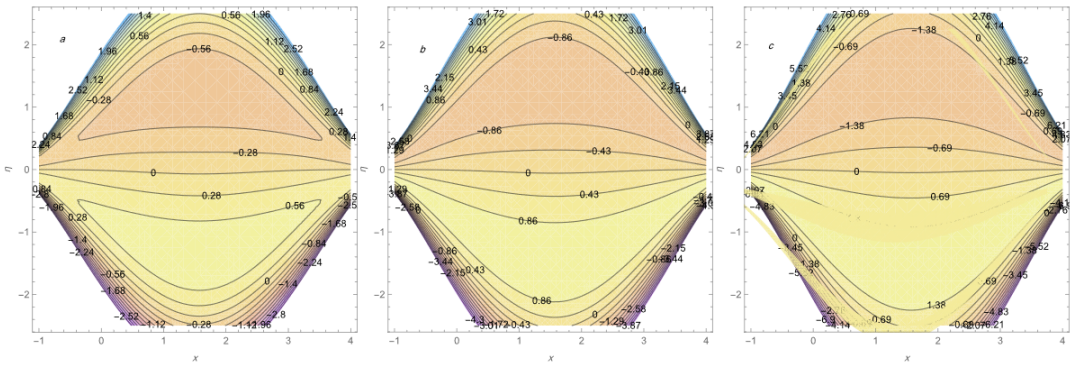

Figure 20: The stream line for F=1,2,3 with ϕ=1, k=25, M=1.

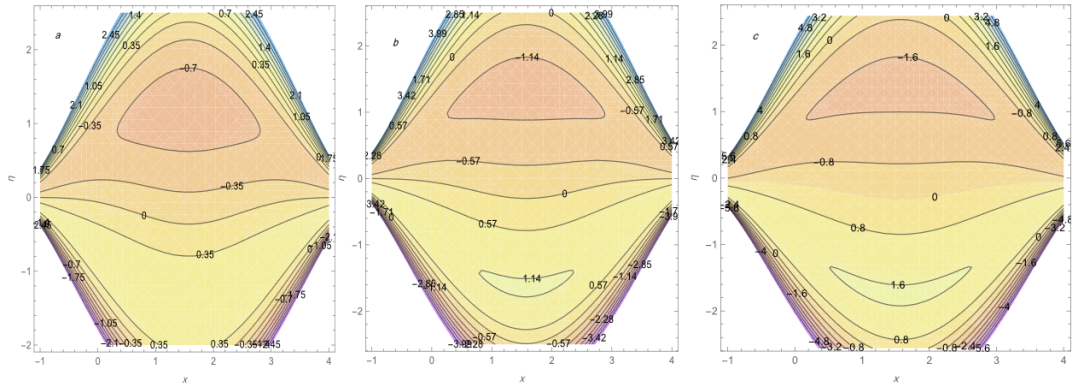

Figure 21: The stream line for F=1,2,3 with ϕ=1, k=5, M=1.

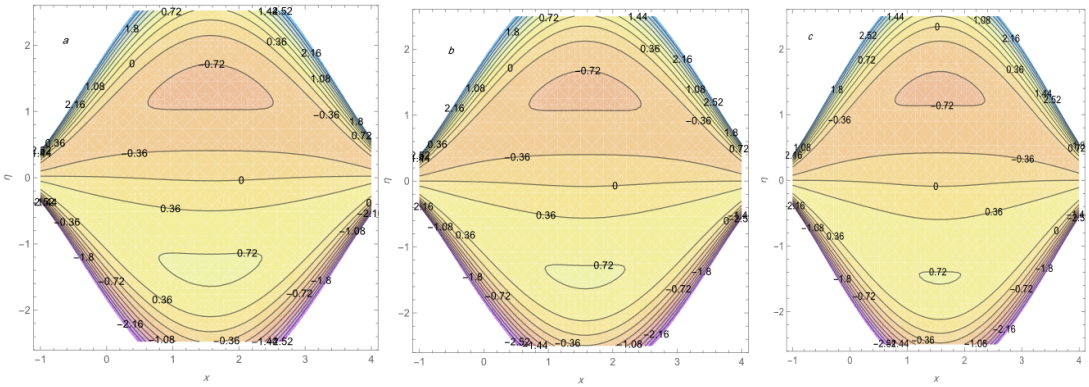

Figure 22: The stream line for M=1,2,3 with ϕ=1, k=25, F=1.

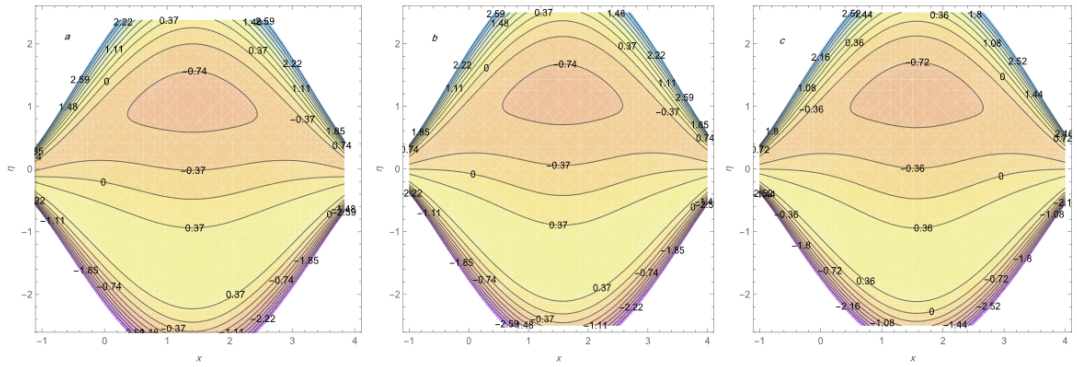

Figure 23: the stream line for M=1,2,3 with ϕ=1, k=5, F=1.

5. Conclusion

This research investigates the peristaltic transport of a Non-Newtonian fluid over a curved tube. This analysis yielded major findings that may be simply summarized as follows:

1. The axial velocity has an upward relationship with both the magnetic field number (Hartman number) and the flow rate F throughout the central region of the tube. Yet, it decreases towards the inner and outer edges of the tube.
2. The magnitude of the pressure gradient $(\frac{\partial p}{\partial x})$ exhibits a drop as the flow rate F and Hartman number rise.
3. From studying the pumping regions, the pumping rate of the peristaltic non-Newtonian fluid declined with a rise in the amplitude ratio parameter and Hartman number parameter.
4. For the small values of k, the boluses are not symmetric in shape and size around the center. While for large values of k, the boluses are symmetric in shape and size around the center. Furthermore, the boluses becoming bigger as the values of ϕ and F increases.

References

[1] K. K. Raju, R. Devanathan, Peristaltic motion of a non-newtonian fluid, Rheologica Acta 11 (2) (1972) 170–178.

[2] K. Kanaka Raju, R. Devanathan, Peristaltic motion of a non-newtonian fluid: Part ii. visco-elastic fluid, Rheologica Acta 13 (1974) 944–948.

[3] L. M. Srivastava, V. P. Srivastava, Peristaltic transport of a non-newtonian fluid: applications to the vas deferens and small intestine, Annals of biomedical engineering 13 (1985) 137–153.

[4] J. Misra, S. Pandey, Peristaltic transport of a non-newtonian fluid with a peripheral layer, International Journal of Engineering Science 37 (14) (1999) 1841–1858.

[5] D. Tsiklauri, I. Beresnev, Non-newtonian effects in the peristaltic flow of a maxwell fluid, Physical Review E 64 (3) (2001) 036303.

[6] A. Medhavi, Peristaltic pumping of a non-newtonian fluid, Applications and Applied Mathematics: An International Journal (AAM) 3 (1) (2008) 12.

[7] N. Ali, M. Sajid, Z. Abbas, T. Javed, Non-newtonian fluid flow induced by peristaltic waves in a curved channel, European Journal of Mechanics-B/Fluids 29 (5) (2010) 387–394.

[8] A. Kalantari, K. Sadeghy, S. Sadeqi, Peristaltic flow of non-newtonian fluids through curved channels: a numerical study, a a 100 (2013) 2.

[9] H. Vaidya, O. D. Makinde, R. Choudhari, K. V. Prasad, S. U. Khan, K. Vajravelu, Peristaltic flow of non-newtonian fluid through an inclined complaint nonlinear tube: application to chyme transport in the gastrointestinal tract, The European Physical Journal Plus 135 (11) (2020) 1–15.

[10] M. A. Murad, A. M. Abdulhadi, Peristaltic transport of power-law fluid in an elastic tapered tube with variable cross-section induced by dilating peristaltic wave, Iraqi Journal of Science 62 (4) (2021) 1293–1306.

[11] D. G. S. Al-Khafajy, A. L. Noor, The peristaltic flow of jeffrey fluid through a flexible channel, Iraqi Journal of Science 63 (12) (2022) 5476–5486.

[12] A. M. Nassief, A. M. Abdulhadi, Influence of magnetic force for peristaltic transport of non-newtonian fluid through porous medium in asymmetric channel, Iraqi Journal of Science 64 (7) (2023) 4467–4486.

[13] N. Ammar, H. A. Ali, Mathematical modelling for peristaltic flow of sutterby fluid through tube under the effect of endoscope, Iraqi Journal of Science 64 (5) (2023) 2368–2381.
[14] W. R. Dean, Fluid motion in a curved channel, Proceedings of the Royal Society of London. Series A, Containing Papers of a Mathematical and Physical Character 121 (787) (1928) 402–420.
[15] W. H. Finlay, J. B. Keller, J. H. Ferziger, Instability and transition in curved channel flow, Journal of Fluid Mechanics 194 (1988) 417–456.
[16] M. A. Leschziner, W. Rodi, Calculation of strongly curved open channel flow, Journal of the Hydraulics Division 105 (10) (1979) 1297–1314.
[17] S. Berger, a. L. Talbot, L. Yao, Flow in curved pipes, Annual review of fluid mechanics 15 (1) (1983) 461–512.
[18] M. Morad, A. Abdul-Hadi, Unsteady flow of non-newtonian fluid in a curved pipe with rectangular cross-section, Iraqi Journal of Science 48 (1) (2007) 182–199.
[19] N. Ali, M. Sajid, Z. Abbas, T. Javed, Non-newtonian fluid flow induced by peristaltic waves in a curved channel, European Journal of Mechanics-B/Fluids 29 (5) (2010) 387–394.
[20] L. F. AL-Juhaishi, M. F. Mohd Ali, H. H. Mohammad, R. K. Ajeel, Numerical thermal-hydraulic performance investigations in turbulent curved channel flow with horseshoe baffles, Heat transfer 49 (6) (2020) 3816–3836.
[21] L. F. M. Al-Juhaishi, M. F. M. Ali, H. H. Mohammad, Numerical study on heat transfer enhancement in a curved channel with baffles, Journal of Advanced Research in Fluid Mechanics and Thermal Sciences 68 (2) (2020) 72–83.
[22] M. Rashid, K. Ansar, S. Nadeem, Effects of induced magnetic field for peristaltic flow of williamson fluid in a curved channel, Physica A: Statistical Mechanics and its Applications 553 (2020) 123979.
[23] A. Abbasi, W. Farooq, E. S. M. Tag-ElDin, S. U. Khan, M. I. Khan, K. Guedri, S. Elattar, M. Waqas, A. M. Galal, Heat transport exploration for hybrid nanoparticle (cu, fe3o4)—based blood flow via tapered complex wavy curved channel with slip features, Micromachines 13 (9) (2022) 1415.
[24] S. Nadeem, N. Abbas, M. Malik, Inspection of hybrid based nanofluid flow over a curved surface, Computer Methods and Programs in Biomedicine 189 (2020) 105193.
[25] A. K. Kempannagari, R. R. Buruju, S. Naramgari, S. Vangala, Effect of joule heating on mhd non-newtonian fluid flow past an exponentially stretching curved surface, Heat Transfer 49 (6) (2020) 3575–3592.
[26] L. Yang, K. Du, A comprehensive review on the natural, forced, and mixed convection of non-newtonian fluids (nanofluids) inside different cavities, Journal of Thermal Analysis and Calorimetry 140 (2020) 2033–2054.
[27] D. H. Ali, M. A. Mohammed, Studying the rheological properties of non-newtonian fluids under the effect of temperature using different chemical additives, Iraqi Journal of Chemical and Petroleum Engineering 21 (2) (2020) 47–56.
[28] A. M. Jasim, A. J. Al-Maliki, New analytical study of non-newtonian jeffery hamel flow of casson fluid in divergent and convergent channels by perturbation iteration algorithm, Basrah Journal of Science 39 (1) (2021) 37–55.
[29] B. Reyes, A. A. Howard, P. Perdikaris, A. M. Tartakovsky, Learning unknown physics of non-newtonian fluids, Physical Review Fluids 6 (7) (2021) 073301.
[30] S. Samrat, Y. Gangadharaiah, G. Ashwinkumar, N. Sandeep, Effect of exponential heat source on parabolic flow of three different non-newtonian fluids, Proceedings of the Institution of Mechanical Engineers, Part E: Journal of Process Mechanical Engineering 236 (5) (2022) 2131–2138.
[31] A. J. Braihi, A. J. Jawad, P. Industrials, Mathematical model analysis of rheology behavior of poly vinyl pyridine (pvp) polymer/iraqi crude oil mixture by using rheocalc program, Test Eng Manag 83 (2020) 21878–21896.
[32] R. Y. Hassen, H. A. Ali, Hall and joule's heating influences on peristaltic transport of bingham plastic fluid with variable viscosity in an inclined tapered asymmetric channel, Ibn AL-Haitham Journal For Pure and Applied Sciences 34 (1) (2021) 68–84.
[33] I. Horiguchi, F. G. Torizal, H. Nagate, H. Inose, K. Inamura, O. Hirata, H. Hayashi, M. Horikawa, Y. Sakai, Protection of human induced pluripotent stem cells against shear stress in suspension culture by bingham plastic fluid, Biotechnology Progress 37 (2) (2021) e3100.
[34] H. N. Mohaisen, A. M. Abdalhadi, Influence of the induced magnetic and rotation on mixed convection heat transfer for the peristaltic transport of bingham plastic fluid in an asymmetric channel, Iraqi Journal of Science 63 (4) (2022) 1770–1785.
[35] M. Khan, T. Salahuddin, M. Awais, M. Altanji, S. Ayub, Q. Khan, Calculating the entropy generation of a bingham plastic fluid flow due to a heated rotating disk, International Communications in Heat and Mass Transfer 143 (2023) 106721.
[36] F. A. Adnan, A. M. A. Hadi, Effect of an inclined magnetic field on peristaltic flow of bingham plastic fluid in an inclined symmetric channel with slip conditions, Iraqi Journal of Science 60 (7) (2019) 1551–1574.
[37] F. A. Adnan, A. M. A. Hadi, peristaltic flow of the bingham plastic fluid in a curved channel, Ibn AL-Haitham Journal For Pure and Applied Sciences 32 (3) (2019) 140–152.
[38] Z. Abbas, R. Mehboob, M. Y. Rafiq, S. Khaliq, A. Ali, Peristaltic pumping of ternary hybrid nanofluid between two sinusoidally deforming curved tubes, Advances in Mechanical Engineering 15 (7) (2023) 1–13.
[39] F. A. Adnan, A. Abdualhadi, Effect of the magnetic field on a peristaltic transport of bingham plastic fluid, Jour. of adv. Research and control 10 (10) (2018) 2007–2024.
[40] D. G. S. Al-Khafajy, J. A. Labban, Temperature and concentration effects on oscillatory flow for variable viscosity carreau fluid through an inclined porous channel, Iraqi Journal of Science (Special Issue 2) (2021) 45–53.
[41] M. Nazeer, Numerical and perturbation solutions of cross flow of an eyring-powell fluid, SN Applied Sciences 3 (2) (2021) 213.
[42] A. S. Kotnurkar, J. Beleri, I. A. Badruddin, K. HMT, S. Kamangar, N. A. Ahammad, Effect of thermal radiation and

double-diffusion convective peristaltic flow of a magneto-jeffrey nanofluid through a flexible channel, Mathematics 10 (10) (2022) 1701.

[43] H. Abdulhussein, A. M. Abdulhadi, The effect of rotation on the heat transfer of a couple stress fluid in a nonuniform inclined asymmetrical channel with inclined mhd, Ibn AL-Haitham Journal For Pure and Applied Sciences 36 (2) (2023) 314–330.

[44] S. G. Lampaert, R. A. van Ostayen, Lubrication theory for bingham plastics, Tribology International 147 (2020) 106160.

[45] A. M. Nassief, A. M. Abdulhadi, Rotation and magnetic force effects on peristaltic transport of non-newtonian fluid in a symmetric channel, Ibn AL-Haitham Journal For Pure and Applied Sciences 36 (2) (2023) 436–453.

[46] K. Panwar, Slip and no slip conditions in serpentine channel for bingham fluid-numerical cfd investigation, Journal of Graphic Era University 11 (1) (2023) 45–56.

[47] M. Khan, T. Salahuddin, M. Awais, M. Altanji, S. Ayub, Q. Khan, Calculating the entropy generation of a bingham plastic fluid flow due to a heated rotating disk, International Communications in Heat and Mass Transfer 143 (2023) 106721.

[48] B. Samanta, G. Das, S. Ray, M. Kaushal, Laminar planar hydraulic jump during free surface flow of bingham plastic liquid, Chemical Engineering Science 284 (2023) 119505.

[49] A. A. Mohammed, L. Z. Hummady, The effect of heat transformation and rotation on sutterby fluid peristaltic flow in an inclined, asymmetric channel with the porousness, Baghdad Science Journal (9) (2023) 13.

[50] A. A. Mohammed, L. Z. Hummady, Influence of heat transform and rotation of sutterby fluid in an asymmetric channel, Iraqi Journal of Science 64 (11) (2023) 5766–5777.